Coverage dependence of the electronic structure of potassium adatoms on the Si(001)-(2×1) surface

H. Ishida and K. Terakura
Institute for Solid State Physics, University of Tokyo, Roppongi, Minato-ku, Tokyo 106, Japan
(Received 1 May 1989; revised manuscript received 31 August 1989)

The electronic structure of potassium adatoms on the Si(001)-(2×1) surface is studied by first-principles calculations within the local-density-functional theory for a wide range of the K coverage (Θ) including low Θ values with negligibly small direct interactions among adatoms. The symmetric dimer model is assumed for the substrate Si which is modeled by a ten-layer slab. As possible adsorption sites for K, a raised site on the Si dimer chain and/or a valley site between two dimer chains are considered. The calculations are performed for Θ ranging from $\frac{1}{6}$ to 1 in units of Si monolayers including the Levine model ($\Theta=\frac{1}{2}$) and also recently proposed double-layer model ($\Theta=1$). No free-electron-like surface band characteristic of the K 4*s* state appears in the Si gap even for higher Θ. However, the two gap states originating from the Si dangling bonds in the limit of $\Theta\rightarrow 0$ shift to higher binding energies by $\sim$0.5 eV with increasing Θ due to the kinetic energy lowering caused by the delocalization of their wave functions toward the overlayer. This is interpreted as a result of the Si-K hybridization which leads to the polarized covalent Si—K bond. The adatom region is essentially neutral even for lower Θ if the charge density is averaged in a K sphere, which implies that the adatom-induced dipole moment to reduce the work function shold be attributed to the adatom polarization due to the Si-K orbital mixing rather than the conventional Θ-dependent charge transfer.

I. INTRODUCTION

Adsorption of alkali metals on metal and semiconductor surfaces has been an active field in surface science for a long time. In its earlier stage,[1–3] large lowering of the substrate work function upon adsorption was the main subject, while recently, subjects such as the appearance of overlayer plasmons,[4–6] coadsorption with molecules such as CO,[7,8] and promotion of catalytic reactions[9,10] have been also intensively studied. A classical picture of Langmuir and Gurney,[11] which was later supported by model theories based on the Anderson Hamiltonian[12–14] and two-step jellium model,[15–18] assumes that the adatom electronic structure changes drastically from a strongly ionic to neutral state with increasing coverage (Θ) due to the depolarization field at adatom sites. On the other hand, recent first-principles calculations performed for alkali-metal overlayers on jellium[19–21] and Al(001) (Ref. 22) surfaces with a wide range of Θ values clarified that the adatom charge state, if simply defined as a number of electrons in an adatom sphere, is very independent of Θ, and that the adatom region is essentially neutral even at low Θ if the electron density is averaged in the atomic sphere. It was proposed that the adatom-substrate bonding is mainly metallic even at low Θ and that the adatom dipole moments should be attributed to polarization of adatoms due to hybridization between adatom and substrate states rather than the conventional Θ-dependent charge transfer. Formation of the polarized covalent adatom-substrate bond was also emphasized by Wimmer, Freeman, Hiskes, and Karo[23–25] for transition-metal substrates such as W and Mo for a high Θ. Their theory was later supported by the experimental work of Soukiassian *et al.*[26] for Cs overlayers on transition metals. The purpose of the present paper is to examine whether such a new picture as deduced from the recent first-principles calculations is also valid for adsorption on semiconductor surfaces. We choose the Si(001)-(2×1) surface as the substrate because adsorption of alkali metals on Si(001)-(2×1) is currently attracting much attention in both experimental and theoretical sides, and is giving rise to controversies on its structural and electronic properties.

On the experimental side, the chain model of Levine[27] in which alkali-metal adatoms form one-dimensional raised chains above the substrate Si dimers had been accepted for a long time as the ordered structure at the saturation Θ (Θ_s). The model corresponds to $\Theta=\frac{1}{2}$ in units of Si monolayers (one adatom per two Si top-layer atoms). Anisotropic plasmon dispersions for the K overlayer measured by Aruga *et al.* with electron-energy-loss spectroscopy (EELS) seemed to support the existence of such one-dimensional metallic chains.[28] On the other hand, a recent photoemission spectroscopy (PES) experiment of Enta *et al.*[29] for the K and Cs overlayers showed that the surface might be semiconducting rather than metallic at Θ_s. Based on the x-ray photoelectron diffraction (XPD) experiment, Abukawa and Kono[30] proposed a new structure model where alkali-metal adatoms form double layers with two kinds of adatom chains: the upper one above the ridge of Si dimers as in Levine model, and additionally the lower one located in the trough between two arrays of Si dimers. Their model corresponds to $\Theta=1$ with two adatom valence electrons per one unit cell, and therefore is compatible with the observed semi-

conducting nature of the overlayer. Very recently, Ichimiya and Kohmoto[31] studied the structure of K/Si(001)-(2×1) by the reflection high-energy electron energy diffraction, and obtained results which favored the double-layer model rather than the Levine model.

On the theoretical side, most of the previous electronic structure calculations for the K/Si(001)-(2×1) surface were performed assuming the Levine model ($\Theta=\frac{1}{2}$), although very recently Batra[32] studied the electronic structure of the double-layer model for the Na overlayer. Ishida *et al.*[33] calculated plasmon dispersions of the K overlayer on Si(001)-(2×1) within the random-phase approximation based on the surface bands calculated with the *DV-Xα* method, and obtained a fair agreement with the EELS experiment of Aruga *et al.*[28] The K charge state estimated by the Mulliken analysis was close to a neutral one. On the other hand, Ciraci and Batra[34,35] performed total-energy and band-structure calculations of the K overlayer using the pseudopotential method. From intactness of the surface band dispersions of the Si(001) dimer states (π and π^* bands) upon K adsorption, it was claimed that K adatoms are completely ionic even at $\Theta=\frac{1}{2}$, and that surface is metallized through partial filling of the Si π^* band rather than formation of metallic K chains. The nearest Si—K bond length found by the total-energy minimization was quite short, and appeared to give a further evidence of the strong ionic adsorption. However, a recent surface-extended x-ray absorption fine-structure study (SEXAFS) experiment by Kendelewicz *et al.*[36] obtained the Si—K bond length (3.14±0.1) Å which was equal to the sum of the covalent radii of K and Si atoms. The underestimation of the Si-K distance in the pseudopotential calculation may result from neglect of the polarization of the 3*p* core states. Using the pseudofunction method, Kasowski and Tsai[37] obtained the Si—K bond length of 3.3 Å for the Levine model which is in agreement with the SEXAFS value. Soukiassian and Kendelewicz[38] studied the core level of Si surface atoms by PES. They found no shift in the binding energy of Si 2*p* upon K adsorption, which suggested that the net charge transfer from the K to Si atoms is quite small. Nishigaki *et al.*[39] studied the surface electronic states of K/Si(001)-(2×1) by metastable deexcitation spectroscopy (MDS). The rapid growth of a sharp peak near the Fermi energy with increasing K coverage was assigned as due to the partially filled K valence states.

In this paper, we present results of the first-principles electronic structure calculations of the K/Si(001)-(2×1) surface in detail for a wide range of Θ values, aiming to provide sound basis which may be useful in discussing the above-mentioned controversial subjects. The present work is, especially, the first that clarifies the adatom electronic structure at low Θ where direct interaction among neighboring adatoms is negligibly small. The lowest Θ in the present work is $\Theta=\frac{1}{6}$, which corresponds to one adatom per six surface Si atoms. It may be indispensable to study the Θ dependence of the adatom electronic structure in a systematic way in order to elucidate whether the K—K bond becomes really metallic at higher Θ.

As for the charge state of adatoms, much of the controversy seems to arise from uncertainty involved in the definition of "ionicity" or "neutrality" of adatoms. Indeed, with a large overlapping between adatom and substrate wave functions, it is impossible to divide the total electron density uniquely into the two parts. The argument of Ciraci and Batra[34,35] that adatoms are perfectly ionic even at $\Theta=\frac{1}{2}$ was mainly based on the absence of surface bands below the Fermi level (E_F) with a parabolic dispersion which exists for isolated monolayers, and also overlayers on simple metals.[40,41] Certainly, the adatom electronic structure on Si(001)-(2×1) is different from that on simple metals owing to the existence of the active Si dangling bonds and the bulk band gap of Si. Even in such a case, as will be shown later, the number of electrons in an adatom sphere, which is related with observable quantities such as work function and core levels, are still very close to that of isolated neutral monolayers. Moreover, detailed analyses of the surface band dispersions and adatom density of states (DOS) suggest the important role of hybridization effects between adatom and substrate states in the adatom-substrate bonding as well as in work-function lowering just as in the case of adsorption on simple metals.[19–22]

The plan of the present paper is as follows. In Sec. II, we describe the overlayer model and method of the calculation. The results and discussions are presented in Sec. III. Summary and Conclusion are given in Sec. IV.

II. OVERLAYER MODEL AND CALCULATIONAL METHOD

The present calculation is performed within the local density approximation in the density functional theory,[42] combined with the norm-conserving pseudopotential,[43] plane-wave basis, and repeating slab geometry. The method is essentially the same as that adopted by Ciraci and Batra,[34,35] except that they used an asymmetric slab where the dangling bonds on the back surface of the substrate Si slab is saturated with hydrogen atoms, whereas we use a symmetric one with an alkali-metal overlayer on each side of the Si slab. We use a ten-layer Si(001) slab as the substrate. Although the asymmetric dimer model may be appropriate for the bare Si(001)-(2×1) surface at room temperatures,[44] the K adsorption will make the dimer more symmetric through the filling of the antibonding surface band as for the dimer bonding. Therefore, the symmetric dimer model is assumed for the structure of the substrate Si(001)-(2×1) surface. We do not consider the relaxation of the surface Si layers, and the nearest neighbor Si—Si bond length, including that of the dimer, is set equal to the bulk value.

We consider two adsorption sites for K atoms as shown in Fig. 1(a). The first one (K_1) is a hollow site between two Si dimers proposed originally by Levine[27] and used in previous theories. Since the pseudopotential calculation without taking account of the K 3*p* state underestimates the Si—K bond length, the Si—K bond length cannot be determined through total-energy minimazation. Recently, Tsukada *et al.*[45] studied the surface band structure of K/Si(001)-(2×1) with the *DV−Xα* method for several values of the Si—K bond

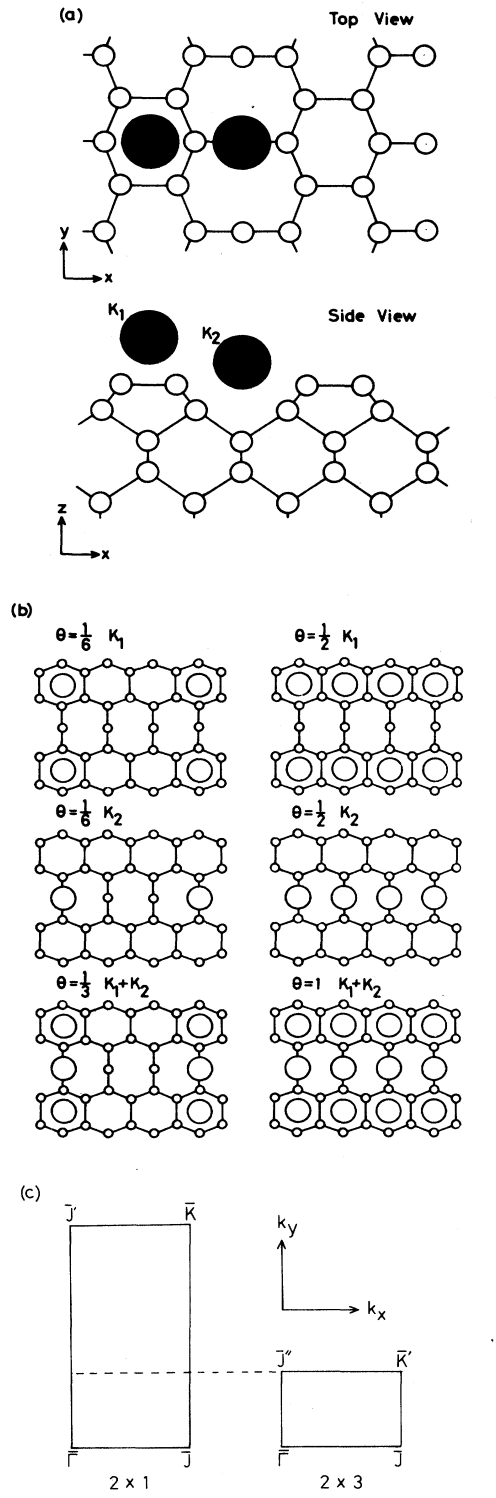

FIG. 1. (a) Adsorption sites of K atoms on the Si(001)-(2×1) surface. The K and Si atoms are indicated by larger and smaller circles, respectively. (b) Six structure models for the K overlayers used in the present calculation with Θ values (adatom coverage) ranging from $\Theta=\frac{1}{6}$ to 1 in units of Si monolayers. (c) Surface Brillouin zone for $\Theta=\frac{1}{2}$ and 1 (left-hand side) and for $\Theta=\frac{1}{6}$ and $\frac{1}{3}$ (right-hand side).

length. Although details of surface bands such as energy separation between two states were slightly affected by changing the bond length, essential parts such as the number of surface states and their overall energy dispersions were rather insensitive to the Si-K distance. Since the emphasis in the present work is placed on studying Θ dependence of the adatom electronic structure in such a way that chemical trends involved are systematically clarified rather than on the quantitative determination of structure parameters, we use the SEXAFS value of 3.14 Å for the Si—K bond length. The second site (K_2) is at a lower position between two dimer chains where K atoms are adsorbed on top of Si atoms in the third layer, as recently proposed by Abukawa and Kono.[30] We use their XPD value of 1.1 Å for the vertical separation between the K_1 and K_2 sites. For the Na adlayer at $\Theta=\frac{1}{2}$, Batra[32] showed that another cave site on top of Si atoms in the fourth layer is energetically more favorable than K_2. Yet, for the case of K, a recent Auger-electron diffraction experiment Asensio *et al.* suggested that adsorption of K atoms takes place at K_2 at room temperature.[46] In any case, quantities such as the surface band dispersion and adatom DOS which we concentrate on in the present work are not very sensitive to the difference in the atomic position between the two sites. Thus we adopt the experimentally proposed K_2 site.

As shown in Fig. 1(b), we calculate the electronic structure of the K overlayers on Si(001)-(2×1) for six overlayer structures with Θ ranging from $\Theta=\frac{1}{6}$ to 1 in units of Si monolayers. They are as follows: (i) K at every third K_1 site ($\Theta=\frac{1}{6}$); (ii) K at every third K_2 site ($\Theta=\frac{1}{6}$); (iii) K at every third K_1 and K_2 sites where it is assumed that K atoms form one-dimensional K chains which are perpendicular to the Si dimer chain (y direction); (iv) K at every K_1 site, i.e., Levine model ($\Theta=\frac{1}{2}$); (v) K at every K_2 site ($\Theta=\frac{1}{2}$); and (vi) K at every K_1 and K_2 sites, i.e., double-layer model. The structures for $\Theta=\frac{1}{6}$ and $\frac{1}{3}$ have the 2×3, while the others have the 2×1 unit cell. The 2×3 overlayer was really observed at low-K coverages, although its atomic structure is still unknown.[29] At $\Theta=\frac{1}{6}$, the distance between neighboring K atoms in the chain direction is equal to 11.49 Å which is sufficiently large to make the orbital overlap between neighboring K atoms negligible.

For estimating the work function accurately, the spacing between two neighboring slabs must be large enough. It is chosen as 16 Å for all the coverages. The electron wave functions are expanded by ~1800 plane waves for $\Theta=\frac{1}{2}$ and 1, and by ~5400 plane waves for $\Theta=\frac{1}{6}$ and $\frac{1}{3}$, where all the bases are used for diagonalizing the Hamiltonian matrix. Although these numbers are not yet sufficient for the perfect convergence of the unoccupied conduction bands, it is sufficient for the convergence of occupied states, and therefore for the charge density and work function. The calculated valence-band width of the ten-layer Si slab, 11.3 eV is in fair agreement with the bulk value, 11.9 eV, calculated with a higher cut-off energy.[47] For $\Theta=\frac{1}{2}$ and 1, the rectangular surface Brilloin zone (SBZ) is divided into 4×8 equal meshes. This leads to 15 independent k points for k-space sampling. Similar

mesh density is used for $\Theta=\frac{1}{6}$ and $\frac{1}{3}$. The iteration procedure is continued until the difference between the input and output surface dipole layers becomes less than 0.15 eV.

III. RESULTS AND DISCUSSIONS

A. Surface electron band structure

Figure 2(a) shows the band structure of the Si(001)-(2×1) surface calculated with the ten-layer slab. The solid and dashed curves represent even and odd states with respect to the symmetry operator about the center plane of the slab, respectively. The energy is measured from the top of the valence bands, and E_F denotes the Fermi energy. The two bands denoted as S_1 and S_2 in the band gap correspond to the bonding π and antibonding π^* surface states which are characteristic of the Si dimer structure. Their dispersions are in good agreement with those in previous calculations.[48,49] Because of the small interaction between the two surfaces of the slab, each S_1 and S_2 splits into a pair of even and odd states with a small energy separation. As is well known, the symmetric dimer model cannot reproduce the semiconductive nature of the surface, and the system becomes metallic with two electrons of the Si dangling bonds accommodated in both S_1 and S_2.

We first show the surface band structures of K/Si(001)-(2×1) for higher Θ ($\Theta=\frac{1}{2}$ and 1), since they have the same SBZ as the bare Si(001)-(2×1), and are easier to study changes of the surface bands upon K adsorption. Figures 2(b), 2(c), and 2(d) show the calculated band structures of K/Si(001)-(2×1) for $\Theta=\frac{1}{2}$ (K_1), $\Theta=\frac{1}{2}$ (K_2), and $\Theta=1$ (K_1+K_2), respectively. The adsorption at K_1 [Figs. 2(b) and 2(d)] gives rise to a third surface state, S_3 in the energy gap region, while this does not occur for the adsorption at K_2. S_3 disperses upward with increasing wave vector, and merges into the bulk conduction bands for larger wave vectors. The two gap states, S_1 and S_2 in Fig. 2(b) (Levine model) correspond to the D_1 and D_2 bands in the calculation of Ciraci and Batra.[34,35] Although the energy location of S_3 is not so far from their R state, as will be shown later, the wave function of S_3 is quite different from that of R which survives even for the bare Si(001), and hence the relation between S_3 and R is not clear at present. (In the calculation of Ciraci and Batra, R merged in the bulk conduction bands

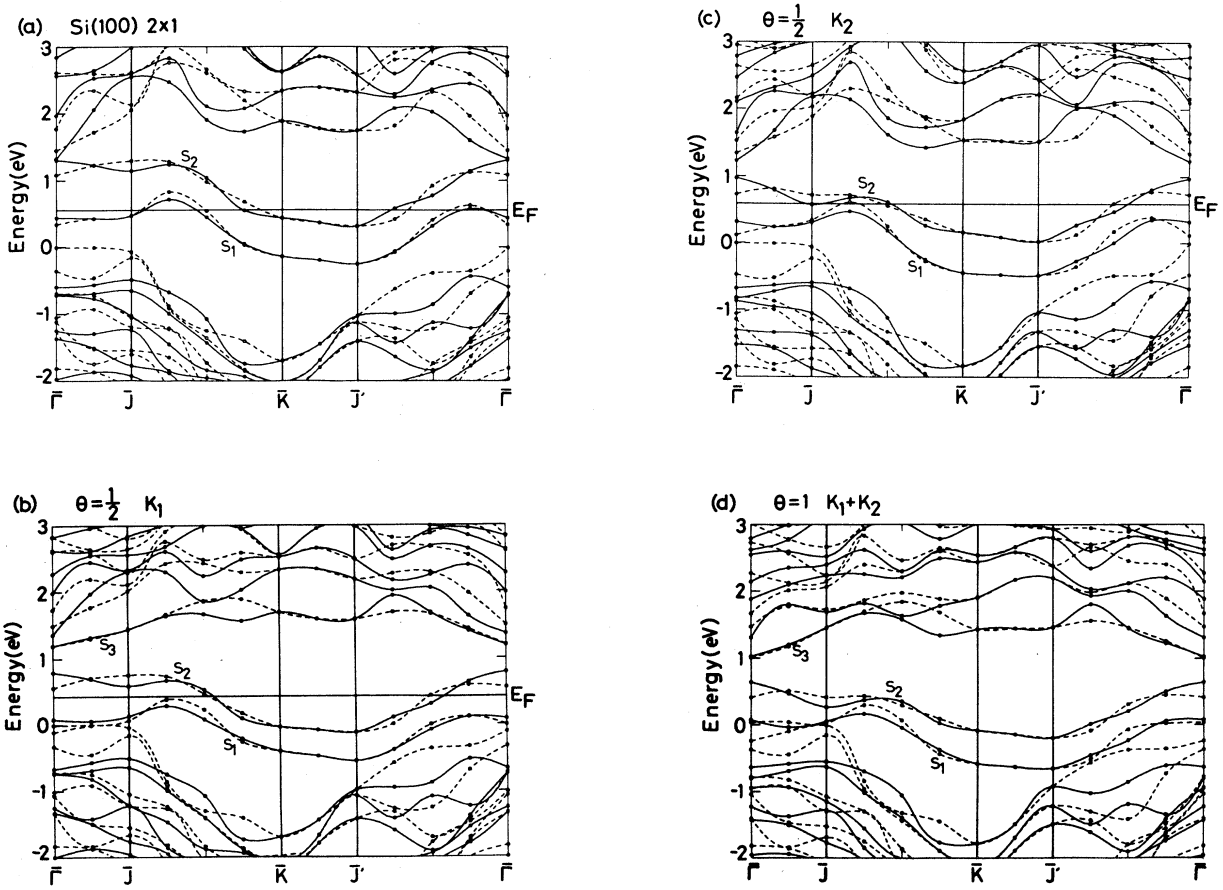

FIG. 2. Calculated surface band structures of K/Si(001)-(2×1) for (a) $\Theta=0$ [bare Si(001) substrate], (b) $\Theta=\frac{1}{2}$ (K_1) (Levine model), (c) $\Theta=\frac{1}{2}$ (K_2), and (d) $\Theta=1$ (double-layer model). The solid and dashed curves indicate even and odd states with respect to symmetry about the center plane of the slab, respectively. E_F denotes the Fermi level.

and was a resonance. Depending on the Si—K bond length, S_3 may also become a resonance.) Because of the difference in the choice of the Si-K distance, the energy separation between S_1 and S_2 along $\bar{\Gamma}$-$\bar{J}'$ and $\bar{J}$-$\bar{K}$ is larger than that between D_1 and D_2.[45] From Fig. 2, it is seen that the overall energy dispersions of S_1 and S_2 are very intact upon K adsorption even at high Θ with rather short K-K distances. No additional free-electron-like K 4*s* band appears in the gap region. This feature was interpreted by Ciraci and Batra as an indication of perfect ionization of K adatoms even at Θ_s, but may be also interpreted as a result of the significant orbital overlapping between Si and K. Indeed, existence of the strong Si pseudopotential may easily modify the free-electron-like K valence bands which originate from the much weaker K pseudopotential.

One important change in the dispersions of S_1 and S_2 upon K adsorption is their shifts to higher binding energies relative to the bulk valence bands in the whole SBZ. The amount of this shift increases with increasing Θ, indicating the larger interaction between the K valence and Si dangling bond states for higher Θ. The shift for $\Theta=1$ amounts to ~ 0.5 eV. Recently, Soukiassian and Kendelewicz[38] studied the valence electronic structure of the Cs and Na covered Si(001)-(2×1) by PES, and found that the occupied surface states shift indeed to higher binding energies with increasing Θ. Their result is in good accord with the present calculation. They interpreted the observed shifts as being due to the Si $3p-Cs$ 6*s* (Si $3p-$Na 3*s*) hybridization. In order to elucidate the origin of the above-mentioned shifts of S_1 and S_2 to higher binding energies, we divide their eigenenergies ε_i into two parts, i.e., the kinetic energy $\varepsilon_{\text{kin}}=\langle\varphi_i|-\Delta/2|\varphi_i\rangle$ and potential energy $\varepsilon_{\text{pot}}=\langle\varphi_i|v|\varphi_i\rangle$, where φ_i is the wave function of the one electron state with energy ε_i, and the potential v includes the Hartree, exchange-correlation, and ion core potentials. The calculated ε_{kin} and ε_{pot} along $\bar{\Gamma}$-$\bar{J}'$ are shown in Fig. 3 for the bare Si(001)-(2×1) (solid lines), Levine model (dashed lines), and double layer model (dotted lines), respectively. From Fig. 3, one can, for instance, see that the energy difference between S_1 and S_2 for the bare Si(001) comes mostly from ε_{pot} rather than ε_{kin}, and also that their downward dispersions along $\bar{\Gamma}-\bar{J}'$ come from the lowering of ε_{kin} with increasing wave vector along the dimer chain direction. Upon K adsorption, the kinetic energies of both states are lowered, although this energy lowering is partly canceled by the increase of ε_{pot}. Therefore, one can conclude that the shifts of S_1 and S_2 to higher binding energies with increasing Θ originates from the lowering of their kinetic energies. Of course, this kinetic energy lowering results from the delocalization of the wave functions of both states toward adatom sites upon K adsorption, which may be interpreted as the Si-K hybridization. On the other hand, a little higher potential energies of both states upon K adsorption reflects the fact that the K cores, toward which their wave functions are partly pulled in, have a less attractive pseudopotential than Si cores. By comparing the results between $\Theta=\frac{1}{2}$ (K_1) and $\Theta=1$ in Fig. 3, it is also seen that ε_{kin} and ε_{pot} of S_1 are not affected very much between $\Theta=\frac{1}{2}$ (K_1) and 1. This

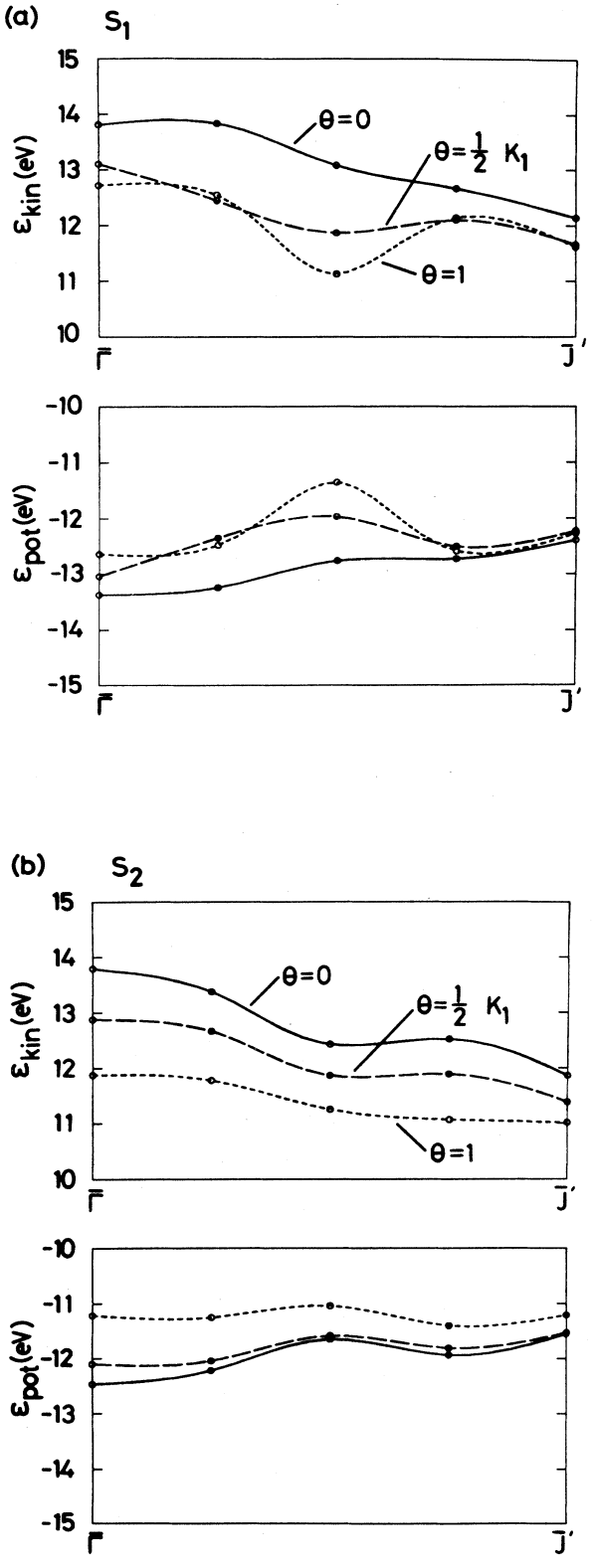

FIG. 3. Kinetic energy contribution ε_{kin} and potential energy contribution ε_{pot} to the one electron energy of (a) S_1 and (b) S_2 states. The solid, dashed, and dotted curves show the calculated results for $\Theta=0$, $\Theta=\frac{1}{2}$ (K_1), and $\Theta=1$ (K_1+K_2), respectively.

implies that the S_1 state which is mainly localized in the raised part of dimer chains interacts strongly with adatoms at K_1, but not so much with adatoms at K_2 in the valley between two dimer chains. On the other hand, S_2, with a larger weight in the valley than S_1 because of its antibonding character with regard to the dimer bonding, interacts strongly also with adatoms at K_2, which then leads to the lowering of $\varepsilon_{\rm kin}$ between $\Theta=\frac{1}{2}$ (K_1) and 1 as much as that between $\Theta=0$ and $\frac{1}{2}$ (K_1).

At $\Theta=1$ (double-layer model), S_1 and S_2 are completely filled and the system becomes semiconducting. This is consistent with the PES experiment of Enta *et al.*[29] and the recent calculation of Batra[32] for the Na overlayer. Very recently, Enta *et al.*[50] performed an angle-resolved PES experiment using a single-domain Si(001)-(2×1) substrate, and observed two occupied surface bands with the energy separation of ~0.8 eV at $\bar{\Gamma}$. Their measured dispersion are in fair agreement with the present result at $\Theta=1$. Nevertheless, we note that Murata *et al.*[51] also performed a PES experiment for K/Si(001)-(2×1) at Θ_s and observed a finite amount of DOS at E_F. Tochihara[52] compared the Auger intensity of the K core state at Θ_s directly with that for K/Cu(001) for which Θ is strictly defined, and claimed that Θ_s is $\Theta=\frac{1}{2}$. Inconsistencies among experiments may arise from difficulty in identifying Θ_s which might depend on sample quality and also crucially on the experimental temperature.

Figures 4(a), 4(b), and 4(c) show the calculated band structures of K/Si(001)-(2×1) for $\Theta=\frac{1}{6}$ (K_1), $\Theta=\frac{1}{6}$ (K_2), and $\Theta=\frac{1}{3}$ (K_1+K_2), respectively. Six surface bands, S_1' to S_6' appear in the gap region, and seven and eight electrons per unit cell are accommodated in them for $\Theta=\frac{1}{6}$ and $\frac{1}{3}$, respectively. Their features are essentially understood in terms of the folding of the S_1 and S_2 bands of Si(001)-(2×1) into a smaller SBZ, plus additional perturbating potentials which split the two bands at zone boundaries.

B. Adatom density of states

In order to study details of the electronic structure of K atoms, we next calculate the adatom DOS as a function of Θ. Figures 5 and 6 show the calculated DOS in a sphere centered at a K atom with a radius equal to 4 a.u. (2.1 Å) for the K_1 and K_2 sites, respectively. The dashed curves in the figures are the corresponding DOS calculated for the bare Si(001)-(2×1), and therefore, the difference between the solid and dashed curves show the states induced in the K sphere upon adsorption. Because of Lorentzian broadening with the width of 0.1 eV used in the actual calculation, the small energy gap between the valence and conduction bands is not clearly seen in Figs. 5 and 6.

One can clearly see the peaks due to S_1 and S_2 (S_1' to S_6' for $\Theta=\frac{1}{3}$ and $\frac{1}{6}$) in the calculated K DOS for both the K_1 and K_2 sites. Their location relative to that at $\Theta=0$ shifts downward with increasing Θ, which is in good accord with the recent PES work[38] as discussed in III A. It is important that these peaks for finite Θ is much enhanced as compared with those for $\Theta=0$. This is espe-

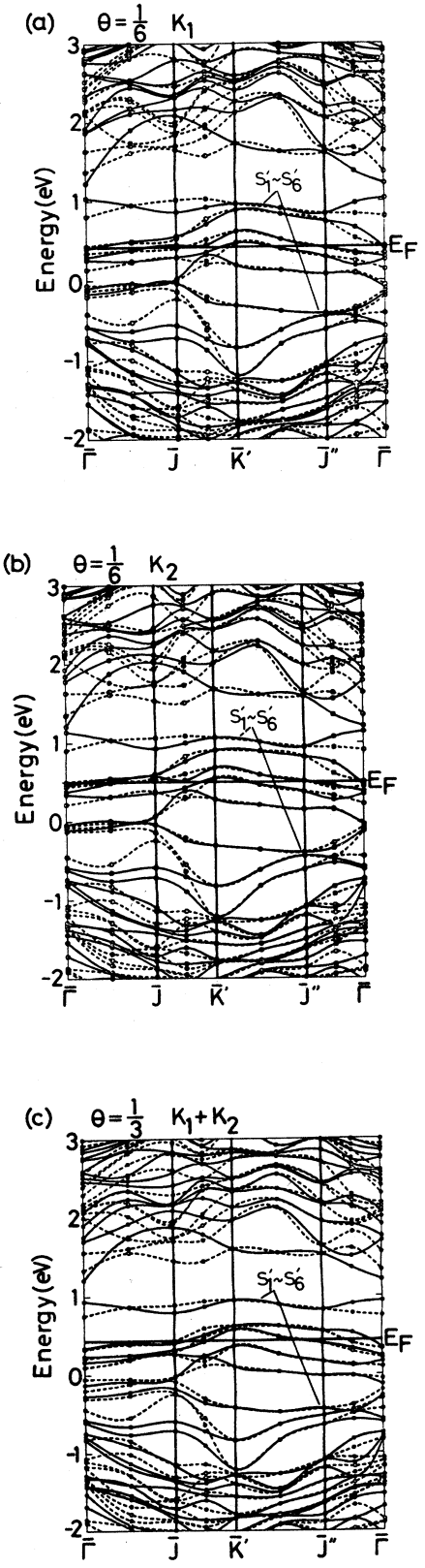

FIG. 4. Calculated surface band structures of K/Si(001)-(2×1) for (a) $\Theta=\frac{1}{6}$ (K_1), (b) $\Theta=\frac{1}{6}$ (K_2), and (c) $\Theta=\frac{1}{3}$ (K_1+K_2).

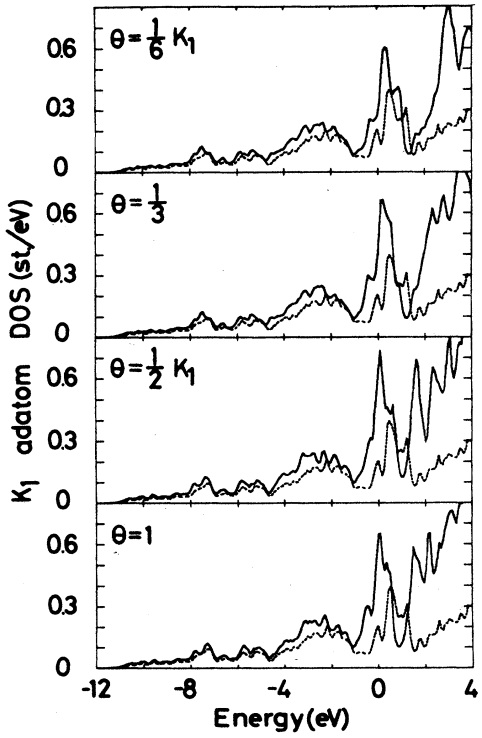

FIG. 5. Calculated adatom density of states (DOS) in a sphere with radius 4 a.u. around the K_1 site as a function of Θ. The dashed curves show DOS in the same sphere for the bare Si(001) surface. The energy is measured from the top of the bulk Si valence bands.

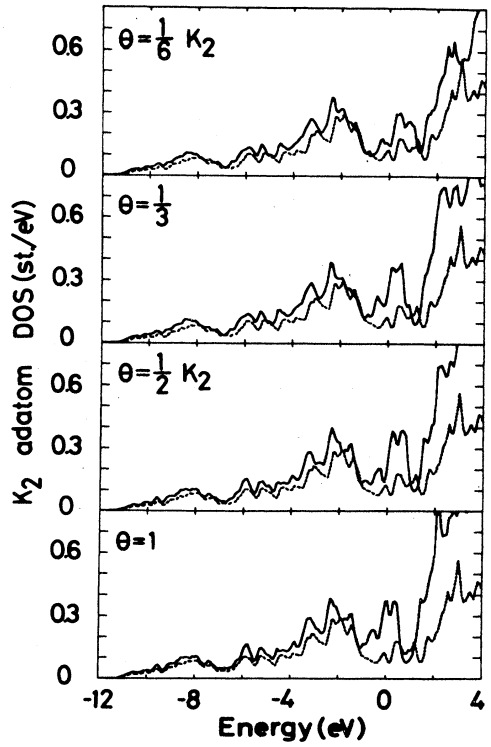

FIG. 6. Calculated adatom DOS in a sphere with radius 4 a.u. around the K_2 site as a function of Θ. The dashed curves show DOS in the same sphere for the bare Si(001) surface.

cially so for the K_2 site. For the bare Si(001)-(2×1) surface, S_1 and S_2 are essentially dangling-bond states of the Si dimers. Therefore their weight at a K_2 site in a cave between two dimer chains is not large, and these two bands do not form sharp peaks in the calculated K_2 DOS. On the other hand, S_1 and S_2 (S_1' to S_6') form distinct peaks in DOS of the K_2 site for finite Θ. Such enhancement in the occupied part of DOS in K spheres may be interpreted as a result of hybridization between the K and Si orbital components. This is supported from the kinetic energy lowering of S_1 and S_2 as was shown in Fig. 3.

Another important message from Figs. 5 and 6 is that the occupied part of DOS in K spheres is rather insensitive to Θ from $\Theta=\frac{1}{6}$ to 1. Such insensitivity of the local DOS and charge state of an atom to the configuration of surrounding atoms was originally put forward by Heine[53] and named "invariance theorem" for impurity atoms in a host metal. Tables I and II list the number of electrons induced in the adatom sphere upon adsorption, n_a as functions of Θ and R for the K_1 and K_2 sites, respectively. (n_a can be evaluated by integrating the difference between the solid and dashed curves in Figs. 5 and 6 up to the Θ-dependent E_F.) The numbers in parentheses are

TABLE I. Number of electrons induced in a K atomic sphere for the K_1 site as functions of the K coverage (Θ) and sphere radius R. The numbers in parentheses indicate the values for the corresponding isolated K layers.

	R (radius of a K sphere) (a.u.)				
Θ	2.0	2.5	3.0	3.5	4.0
$\frac{1}{6}$	0.013	0.047	0.119	0.235	0.388
(K_1)	(0.020)	(0.057)	(0.122)	(0.215)	(0.324)
$\frac{1}{3}$	0.018	0.062	0.153	0.297	0.494
$\frac{1}{2}$	0.013	0.067	0.165	0.321	0.533
(K_1)	(0.028)	(0.081)	(0.179)	(0.326)	(0.510)
1	0.020	0.072	0.180	0.358	0.611

TABLE II. Number of electrons induced in a K atomic sphere for the K_2 site as functions of the K coverage (Θ) and sphere radius R. The numbers in parentheses indicate the values for the corresponding isolated K layers.

	R (radius of a K sphere) (a.u.)				
Θ	2.0	2.5	3.0	3.5	4.0
$\frac{1}{6}$	0.013	0.049	0.122	0.237	0.386
(K_2)	(0.021)	(0.057)	(0.122)	(0.213)	(0.320)
$\frac{1}{3}$	0.016	0.060	0.147	0.286	0.474
$\frac{1}{2}$	0.022	0.063	0.155	0.304	0.503
(K_2)	(0.028)	(0.081)	(0.179)	(0.325)	(0.508)
1	0.021	0.074	0.180	0.355	0.598

the electron numbers in the same sphere calculated for isolated K monolayers with the same overlayer structure, n_a^{iso}. (The electronic structure of isolated K layers was calculated only for $\Theta=\frac{1}{6}$ and $\frac{1}{2}$.) The calculated n_a becomes larger with increasing Θ, reflecting the increase of the K atomic density. However, most important is the fact that n_a is close to, and even larger than n_a^{iso} for $R \geq 3.5$ a.u. (1.85 Å) regardless of Θ. Hence, the adatom region is essentially neutral even at low Θ if the electron density is averaged over the atomic sphere. On the other hand, the dipole part of the electron density is strongly modified in a K sphere and leads to the large dipole moment to reduce the work function, as will be discussed later.

In Figs. 5 and 6, there is a large increase of the K DOS in a wide energy region of the Si conduction bands. This is, of course, due to the unoccupied part of the K valence states which exists as resonances in the host conduction bands. Such resonant states cannot be so obviously identified in the energy dispersion curves shown in III A. The width of these resonant bands becomes larger with increasing Θ due to the larger overlapping among neighboring adatom orbitals, and for the K_1 site, its lower edge appears in the gap region as S_3 for $\Theta=\frac{1}{2}$ and 1 as discussed before.

In order to examine more details of the K valence states, we next study the partial DOS of K adatoms for $\Theta=\frac{1}{2}$ and 1. Figures 7(a)–7(d) show the calculated s, p_x

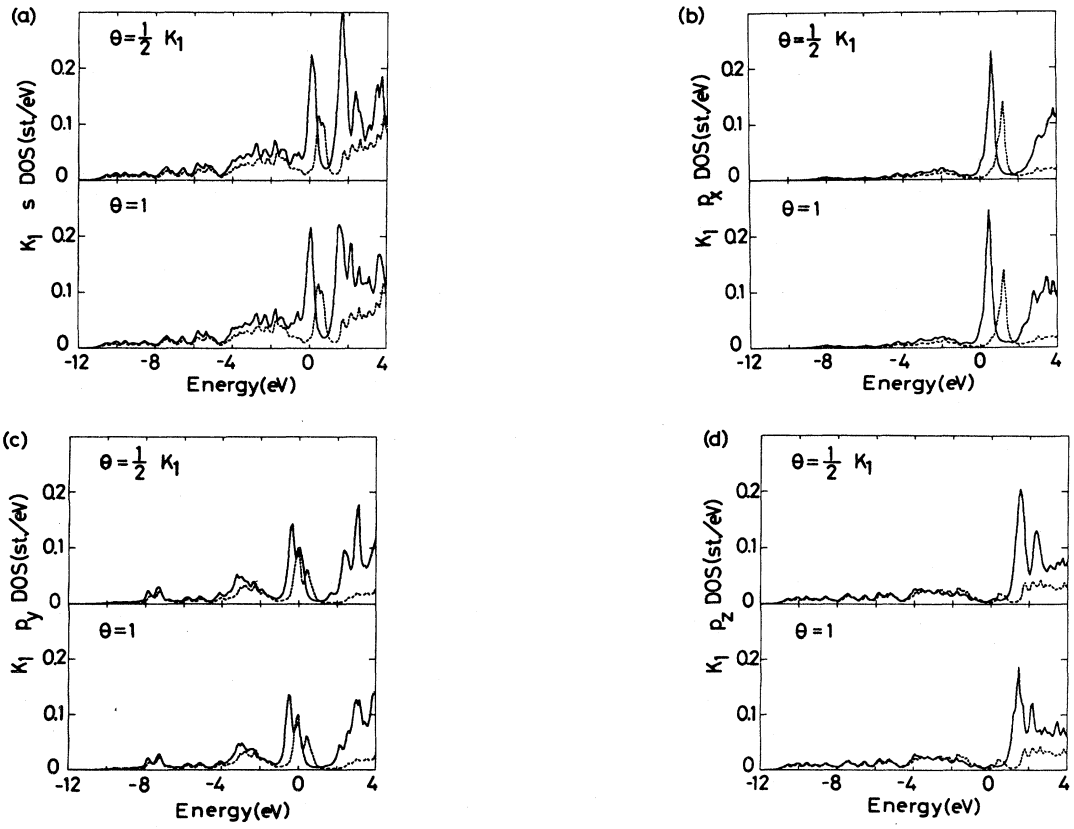

FIG. 7. The calculated partial DOS of a K atom at the K_1 site for $\Theta=\frac{1}{2}$ (K_1) and 1. (a) s, (b) p_x, (c) p_y, and (d) p_z components. The dashed curves show the results for $\Theta=0$.

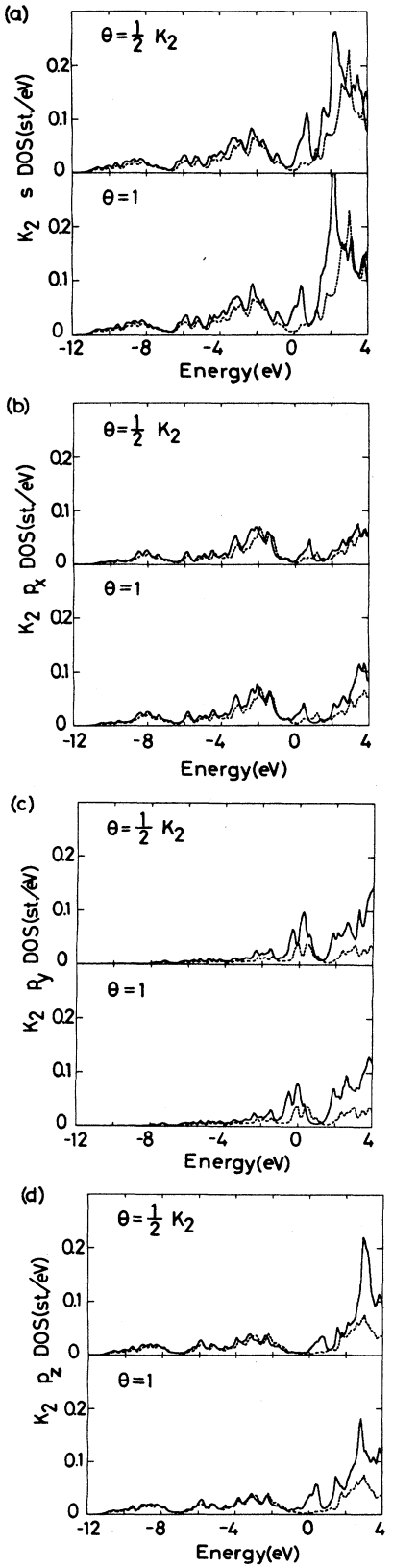

FIG. 8. The calculated partial DOS of a K atom at the K_2 site for $\Theta=\frac{1}{2}$ (K_2) and 1. (a) s, (b) p_x, (c) p_y, and (d) p_z components. The dashed curves show the results for $\Theta=0$.

(dimer bond direction), p_y (chain direction), and p_z DOS in a K sphere for the K_1 site with the same radius as Fig. 5, respectively. Here the dashed curves in these figures give the partial DOS in the same K sphere for the bare Si(001)-(2×1). The occupied part of the calculated partial DOS is seen again as rather insensitive to Θ as in the case of the total K DOS. Because of symmetry K 4s mainly hybridizes with the π orbital of Si dimers around $\bar{\Gamma}$-$\bar{J}$ in SBZ, and form a sharp peak at a position corresponding to the energy of S_1 near $\bar{\Gamma}$-$\bar{J}$. In the same way, K 4p_y and 4p_x mainly hybridize with the π (around $\bar{J}'$-$\bar{K}$) and π^* (around $\bar{\Gamma}$-$\bar{J}$) of Si dimers, and give rise to peaks in S_1 and S_2, respectively. Partial occupation of the p_x and p_y states below E_F results in the decrease in the occupation of K 4s as compared with those for corresponding isolated K layers. Nevertheless, the sum of occupation numbers over all the orbital components is affected very little as emphasized before. In contrast to 4p_x and 4p_y, K 4p_z is mostly unoccupied, and contributes to the unoccupied part of the K DOS. Therefore, the strong modification of the dipole part of the electron density in a K sphere which results in the adatom dipole moment is due to the mixing of the Si and K states rather than the intraatomic polarization (K 4s-4p_z mixing). It is seen that S_3 is a hybridized peak of K 4s and 4p_z. As will be shown later, S_3 is an antibonding state regarding the adatom-substrate bonding whose wave function strongly polarizes toward the vacuum side of K atoms.

Figures 8(a)–8(d) are the calculated partial DOS (PDOS) for the K_2 site. Owing to the different symmetry, the $\mathbf{k}_\parallel$ space in SBZ, where each component of adatom states couples with the π and π^* dimer orbitals, changes from the corresponding one for the K_1 site. For example, K 4s couples with π around $\bar{\Gamma}$ and also with π^* around $\bar{J}$ in SBZ. As a result, the peak position in the s PDOS coincides with the energy of S_2 near $\bar{J}$ rather than that of S_1 near $\bar{\Gamma}$. Another interesting feature may be the fact that K 4p_z contributes also to S_1 and S_2 states and gets partly filled in contrast to the case of the K_1 adsorption and also adsorption of alkali metals on flat surfaces of simple metals.[20,22] Such a difference may be the geometrical effect which reflects the adsorption in the valley site.

C. Charge density plot of surface states

In order to illustrate modifications of surface-state wave functions upon K adsorption more clearly, we next analyze their change densities. In Fig. 9(a), we show contour plots of the charge densities of S_1, S_2, and S_3 at $\bar{\Gamma}$ for the Levine model[27] ($\Theta=\frac{1}{2}$). The vertical cut plane is perpendicular to the dimer chain direction, and passes through the midpoint of a nearest Si—K bond as shown in the inset. The solid circles indicate the projection of Si and K atoms onto the plane, and there are actually no atoms on it. The corresponding charge density plots for the bare Si(001)-(2×1) are given in Fig. 9(b), where it is demonstrated that S_1 and S_2 originate from the two dangling bonds of Si dimers. By comparing the two figures, one can observe contribution of K 4s to S_1 for Fig. 9(a);

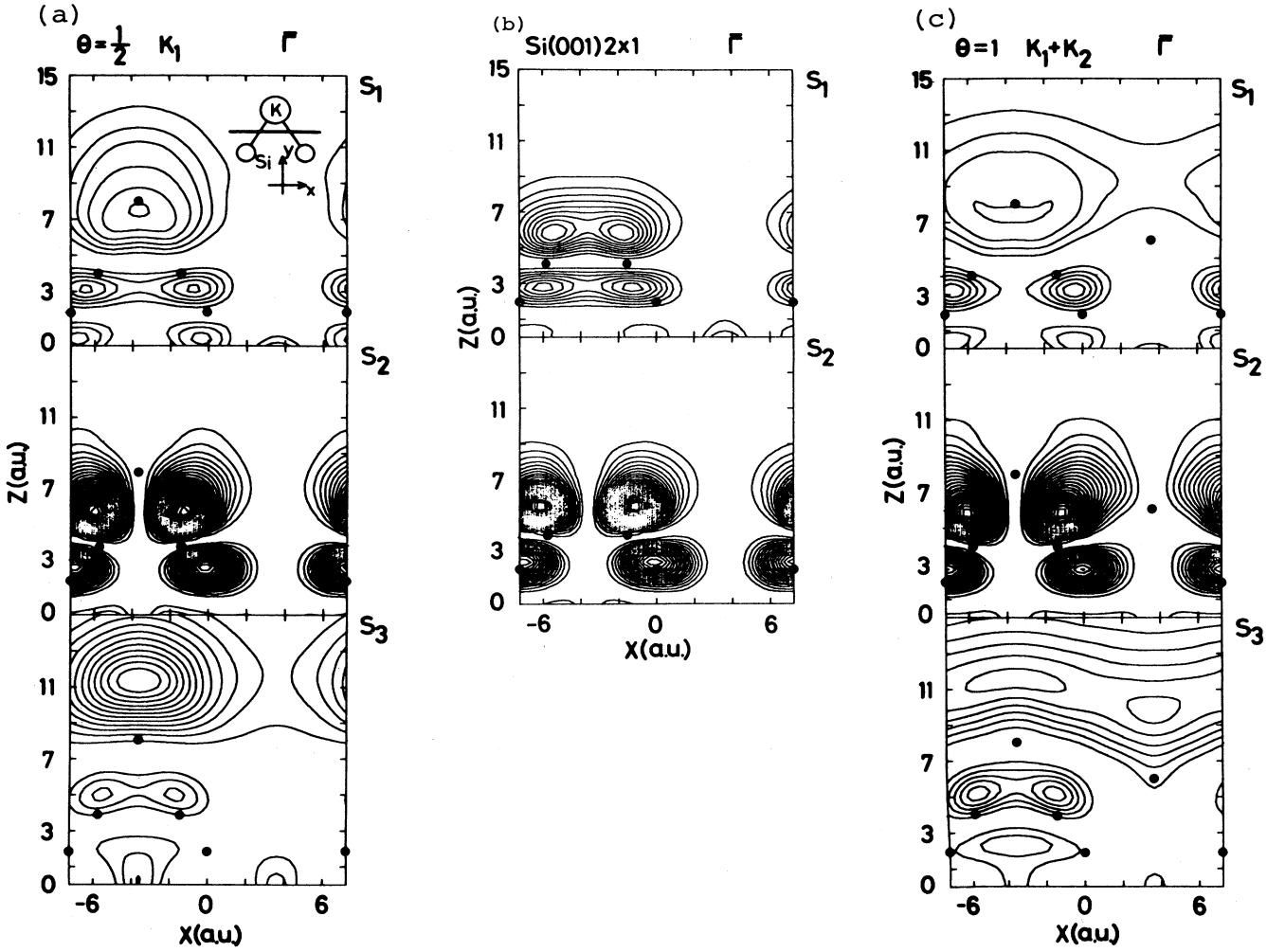

FIG. 9. Charge-density contour plots of S_1, S_2, and S_3 at $\bar{\Gamma}$ for (a) $\Theta=\frac{1}{2}$ (Levine model), (b) the bare Si(001) surface, and (c) $\Theta=1$ (double-layer model). The vertical cut plane passes the midpoint of the nearest Si—K bond and is perpendicular to the Si dimer chain. The contour spacings are the same for all the panels.

charge plots of S_1 for the bare Si(001) have two maxima in the vacuum side of a dimer due to the two Si dangling-bond orbitals, while there is only one broad maximum characteristic of K 4s in the corresponding one for the K covered surface. Modifications of the S_2 wave function at $\bar{\Gamma}$ on the plane is smaller than that of S_1, yet, it is still seen that its tail is extended toward the vacuum side to some degree. As is seen from Fig. 3, the kinetic energy lowering between $\Theta=0$ and $\frac{1}{2}$ (K_1) is 0.7–0.8 eV for both S_1 and S_2, and thus, although not so clear in Fig. 9(a), the wave function of S_2 is also delocalized upon K adsorption as much as S_1. Ciraci and Batra[34,35] showed similar charge-density plots of S_1 and S_2 for both the bare and K covered Si(001)-(2×1) surfaces. No qualitative change characteristic of K 4s was observed in the S_1 charge density upon K adsorption, and this fact was emphasized as a supporting evidence of their conclusion that there is no contribution of K valence states to S_1 and S_2. Their results are at variance with ours. The discrepancy may come from difference in the choice of the wave vector $\mathbf{k}_\parallel$ between theirs and ours. Due to symmetry of the K_1 site, the coupling between the K 4s and Si dangling-bond states becomes smaller with the increase of $\mathbf{k}_\parallel$ in the chain direction, which then leads to smaller contribution of K 4s to S_1. We showed the charge plots at $\bar{\Gamma}$ where the Si π–K 4s coupling becomes the largest, while they showed those at $\mathbf{k}_\parallel=(0,0.291)$ Å^{-1} where the coupling may be appreciably reduced. Nevertheless, as is seen from Fig. 3, the kinetic energy of S_1 is reduced even for such a $\mathbf{k}_\parallel$ point as much as at $\bar{\Gamma}$ because of the coupling with higher K states rather than K 4s. Figure 9(a) shows that S_3 is an antibonding state as to the Si—K bonding whose wave function is strongly polarized toward the vacuum side of a K atom; its charge density takes a maximum value at a position shifted from the K ion core by ~3 a.u. (1.59 Å) toward the vacuum. As stat-

ed before, such a wave function is described as a mixed state of K $4s$ and $4p_z$. Existence of such a strong antibonding surface (or resonant) state above E_F has been established for alkali-metal adatoms on simple metal substrates, and hence may be a common characteristic feature of alkali-metal adsorption systems independent of the species of substrates.[20,21]

Here we briefly discuss the origin of the energy-loss peak observed in the EELS experiment of Aruga *et al.*[28] Ciraci and Batra[34,35] assigned the peak to an individual excitation from S_1 to a resonance, R (in their notation) which exists even for the bare Si(001)-(2×1) surface. However, the following two observations that (i) the intensity of the peak rapidly grows above some critical K coverage, and that (ii) similar energy-less peaks roughly with the same energies have been reported for the K monolayers on several other metal substrates[4] suggest strongly that the peak is really related with the excitation among K valence states. As stated in the above, the common characteristics of the alkali-metal adatom electronic structure is the existence of partially occupied valence s-like states hybridized with substrate orbitals and unoccupied antibonding states made by the mixing of valence s and p_z orbitals. (They correspond to S_1 and S_3 for the present case.) Since the excitation from S_1 to S_3 induces a vertical dipole moment which strongly interacts with incoming electrons,[54] it is expected that the excitation may give rise to a sharp peak in EELS experiments. In the present case, the energy difference between S_1 and S_3 at $\bar{\Gamma}$ is ~ 1.2 eV. Although this value is somewhat smaller than the experimental value ~ 1.7 eV at $\bar{\Gamma}$, it is possible that the loss energy is increased from the individual excitation energy by the plasmon field. As to the question of whether the peak is individual or collective (plasmon), there is still a little ambiguity. The energy of interband plasmons is a sum of the individual excitation energy and an additional energy due to the dipole field of the excitation.[55,56] It was shown by Ishida *et al.*[33] and by Nakayama *et al.*[55] that the latter contribution to the interband plasmon between the valence s- and p_z-like states shows a negative linear dependence as a function of $\mathbf{k}_\parallel$. On the other hand, the observed energy loss showed a positive linear dependence with increasing $\mathbf{k}_\parallel$. Nevertheless, this apparent inconsistency alone would not necessarily negate the possibility of the interband plasmon, since if the increase in the individual excitation energy with increasing $\mathbf{k}_\parallel$ surpasses the contribution of the plasmon field, the total disperson might reproduce the observed positive linear dispersion.

Figure 9(c) shows the charge-density plots of S_1, S_2, and S_3 for the double-layer model ($\Theta=1$) at $\bar{\Gamma}$. The contour plot for S_1 again shows the contribution of $4s$ of K atoms at the K_1 site. The charge density of S_2 is more extended toward the overlayer region than that for Levine model, indicating larger hybridization with adatom states. S_3 is again an antibonding state whose amplitude is dominated by that in the vacuum side of both the K_1 and K_2 sites. In Fig. 9(c), the contribution of the K_2 $4s$ orbital to the surface states is not clearly seen. As stated before, the $4s$ state of K atoms at K_2 mainly hybridizes with S_2 near $\bar{J}$ in SBZ. Figure 10(a) shows the charge plots of S_1 and S_2 at $\bar{J}$ at $\Theta=\frac{1}{2}$ with adatoms at K_2. The corresponding plots for the bare Si(001) are given in Fig. 10(c). The large enhancement in the amplitude of S_2 near the K_2 site upon K adsorption demonstrates the important role of the K_2 $4s$ state to S_2. The hybridization of K_2 $4s$ with Si dangling-bond states is also seen in the energy dispersion of S_2 along $\bar{\Gamma}$-$\bar{J}$; its downward dispersion along $\bar{\Gamma}$-$\bar{J}$ for the overlayers with adatoms at K_2 [Figs. 2(c) and 2(d)] is considerably larger than those without adatoms at K_2 [Figs. 2(a) and 2(b)].

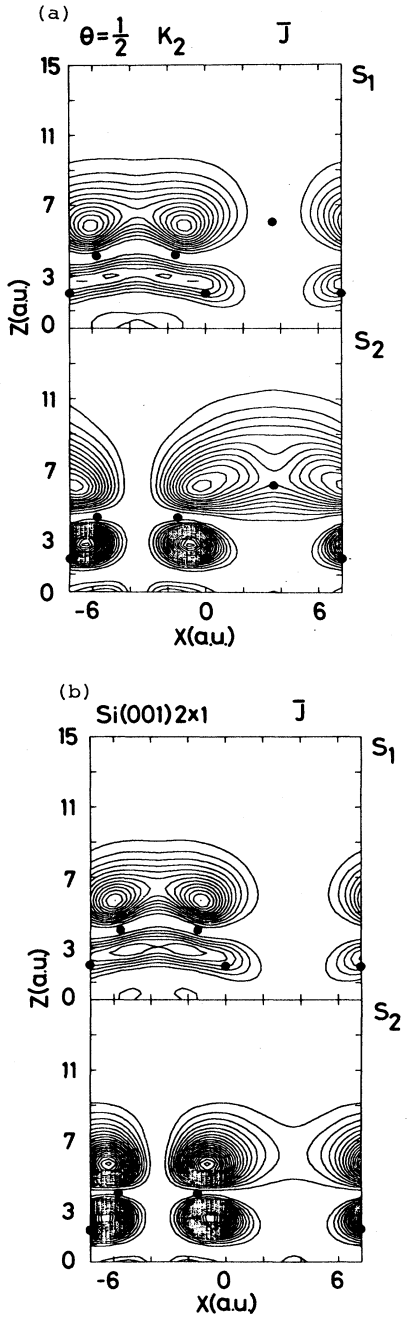

FIG. 10. Charge-density contour plots of S_1 and S_2 at $\bar{J}$ for (a) $\Theta=\frac{1}{2}$ (K_2) and (b) the bare Si(001) surface. The vertical cut plane and the contour spacing are the same as in Fig. 9.

D. Difference charge and work-function change

Next, we discuss the redistribution of the total electron density due to the Si-K interaction which leads to the well-known Θ-dependent work-function change, $\Delta\Phi(\Theta)$. For many metal substrates, it is well known that the substrate work function is almost linearly reduced as a function of Θ for lower Θ, while for higher Θ, after taking a shallow minimum value at some Θ, it slowly rises to a saturation value characteristic of the work function of bulk alkali metals.[56] Since $\Delta\Phi(\Theta)$ is proportional to the adatom-induced dipole moment per adatom, $d(\Theta)$ times Θ, the above-mentioned Θ dependence means that $d(\Theta)$ is greatly reduced with increasing Θ. Recently, it was pointed out explicitly[20] that $d(\Theta)$ has two contributions and is written as

$$d(\Theta)=D(1-\sum_a \langle C_a^\dagger C_a \rangle)+\sum_{ab}\mu_{ab}\langle C_a^\dagger C_b \rangle+\text{c.c.}\ , \qquad (1)$$

where a and b denote the adatom and substrate states, and D and μ_{ab} are dipole matrix elements. The first is the conventional charge-transfer term, while the second comes from the polarization of adatoms due to hybridization between adatom and substate states. According to the recent analyses for simple metal substrates based on the first-principles calculations,[20-22] the second contribution plays a dominant role in the Θ dependence of $d(\Theta)$ in contrast to the classical Gurney model.[11] This was further substantiated by the observation of the close correlation between the decrease of $d(\Theta)$ and weakening of the adatom-substrate bonding with increasing Θ.

Because the electron density of the bulk K is much smaller than that of Si, the total electron density itself is not very meaningful in studying the change in the surface charge density. Instead, we show the difference charge, $\delta\rho(\mathbf{r},\Theta)$ which is defined as the total electron density of K/Si(001) minus the superposed density of the bare Si(001)-(2×1) and isolated K monolayer. For example, the electrostatic potential change, $\delta\varphi(\mathbf{r},\Theta)$ associated with $\delta\rho(\mathbf{r},\Theta)$ gives the change in the surface potential barrier upon K adsorption, and therefore the difference between its value at the vacuum and that in the bulk is equal to $\Delta\Phi(\Theta)$.

Figure 11 shows the contour plots of the difference charge $\delta\rho(\mathbf{r},\Theta)$ at $\Theta=\frac{1}{6}$ (K_1), $\frac{1}{6}$ (K_2), and $\frac{1}{3}$ (K_1+K_2). For $\Theta=\frac{1}{3}$, $\delta\rho(\mathbf{r},\Theta)$ is defined as the charge density of K/Si(001) minus the superposed density of the three surfaces, i.e., the bare Si(001), the unsupported overlayer at $\Theta=\frac{1}{6}$ for the K_1 site, and also that for the K_2 site. The vertical cut plane for Figs. 11(a), 11(c) and 11(e) is the same as for Figs. 9–10, while that for Figs. 11(b) and 11(f) is parallel to the dimer chain direction and contains adatoms at every third K_1 site. The vertical cut plane for Fig. 11(d) is also parallel to the dimer chain, but contains adatoms at K_2 sites. The contour spacing is 0.0005 a.u., and the solid, dot-dashed, and dashed curves correspond to positive, zero, and negative values of $\delta\rho(\mathbf{r},\Theta)$, respectively. The kidney-shaped charge depletion in the vacuum side of K atoms is a characteristic feature of alkali-metal adatoms at lower Θ,[57] and also observed in previous calculations with simple metal substrates.[19-22] The charge depletion in the vacuum side of a K atom at K_1 has an almost semispherical shape, which shows that the interaction between neighboring K atoms in the dimer chain direction is quite small. The corresponding charge depletion for the K_2 site is a little more stretched in the vertical direction, and simultaneously more compressed in the dimer bond direction because of its smaller vertical separation from the Si dimer atoms. The charge depletion areas appear not only in the vacuum side of K atoms but also in the bulk side of Si dimers. Because the charge depletion in the K side is spacially much more extended than that in the Si side, the adatom-induced dipole moment which emphasizes the spacial extension of $\delta\rho(\mathbf{r},\Theta)$ besides its amplitude has the sign to lower the work function. However, the negative amplitude of

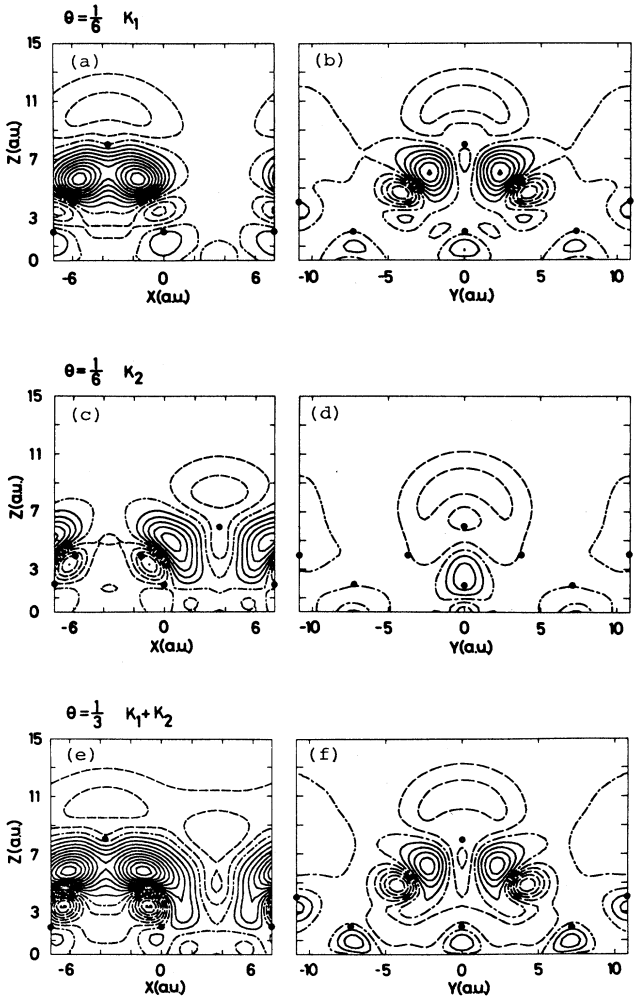

FIG. 11. Contour maps of the difference charge $\delta\rho(\mathbf{r},\Theta)$ for (a) and (b) $\Theta=\frac{1}{6}$ (K_1), (c) and (d) $\Theta=\frac{1}{6}$ (K_2), and (e) and (f) $\Theta=\frac{1}{3}$ (K_1+K_2). The contour spacings are 0.0005 a.u., and the solid, dashed, and dot-dashed curves indicate positive, negative, and zero values of $\delta\rho(\mathbf{r},\Theta)$, respectively. The vertical cut planes for (a), (c), and (e) are the same as that in Fig. 9. The cut planes for (b), (d), and (f) are parallel to the dimer chain and contain adatoms at every third K_1 or K_2 site.

$\delta\rho(\mathbf{r},\Theta)$ in the Si side itself is as much as that in the K side. On the other hand, the main charge accumulation appears in the Si-K interface; there is a maximum in the calculated $\delta\rho(\mathbf{r},\Theta)$ for each Si—K bond. The adatoms at K_1 mainly form chemical bonds with the Si dimer atoms, while the bond charge contour for the adatoms at K_2 suggests that the second layer Si atoms also contribute to the Si-K bonding for the K_2 adsorption.

The difference charge maps for higher Θ ($\Theta=\frac{1}{2}$ and 1) are shown in Fig. 12. The cut plane for each panel is the same as the corresponding one in Fig. 11. Qualitative features of $\delta\rho(\mathbf{r},\Theta)$ in Fig. 12 are essentially the same as those for lower Θ; the charge depletion areas appear on the vacuum side of K adatoms and also the bulk side of Si dimers, whereas bond charges are formed in the Si-K interface for each Si—K bond. Yet, looking into more details, one notices a certain degree of Θ dependence which reflects the larger K-K interaction for higher Θ. The amplitude of the bond charge in the Si—K bond for $\Theta=\frac{1}{2}$ and 1 is a little smaller than those for lower Θ, and also the kidney-shaped charge depletion in the vacuum side of K atoms is considerably shrinked for higher Θ. These signify the weaker Si—K bonding, and consequently smaller polarization of K atoms with increasing Θ. it should be also remarked that the largest charge depletion area on the K side for higher Θ appears around the middle of neighboring K atoms at the cost of some K—K bond charge instead of just on the vacuum side of an adatom for lower Θ [compare Figs. 11(b) and 12(b)].

Next we discuss the work-function change $\Delta\Phi(\Theta)$ for the present system. Figures 13(a) and 13(b) show $\delta\varphi(\mathbf{r},\Theta)$ along the vertical axis containing a K atom at the K_1 and K_2 sites, respectively. The K atomic position is indicated by a small arrow. $\delta\varphi(\mathbf{r},\Theta)$ almost vanishes at only a few layers inside the Si substrate, which shows that the Si substrate can screen the adatom dipole field quite efficiently. Due to the dipole layer formed by the bond charge in the Si-K interface and charge depletion areas in the K side, the value of $\delta\varphi(\mathbf{r},\Theta)$ at the vacuum is lower than that in the bulk, which thus results in reduction of the potential barrier for outgoing electrons and gives $\Delta\Phi(\Theta)$. $\Delta\Phi(\Theta)$ evaluated from the values of $\delta\varphi(\mathbf{r},\Theta)$ at the vacuum is summarized in Fig. 14. These values may give us some hints for assigning the adsorption site of K atoms. The work function of the present system was measured by several groups. In contrast to the case of metal substrates, the measured $\Delta\Phi(\Theta)$ showed only a small or, depending on the experimental condition, even no minimum value before Θ_s. $\Delta\Phi(\Theta)$ at Θ_s measured by

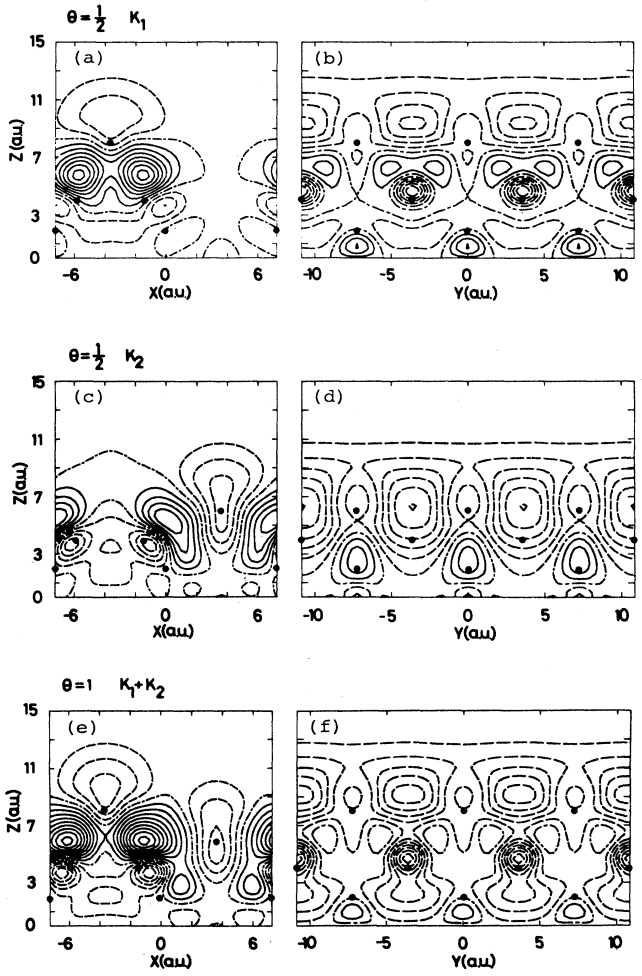

FIG. 12. Contour maps of the difference charge $\delta\rho(\mathbf{r},\Theta)$ for (a) and (b) $\Theta=\frac{1}{2}$ (K_1), (c) and (d) $\Theta=\frac{1}{2}$ (K_2), and (e) and (f) $\Theta=1$ (K_1+K_2). The contour spacing and vertical cut planes are the same as those in Fig. 11.

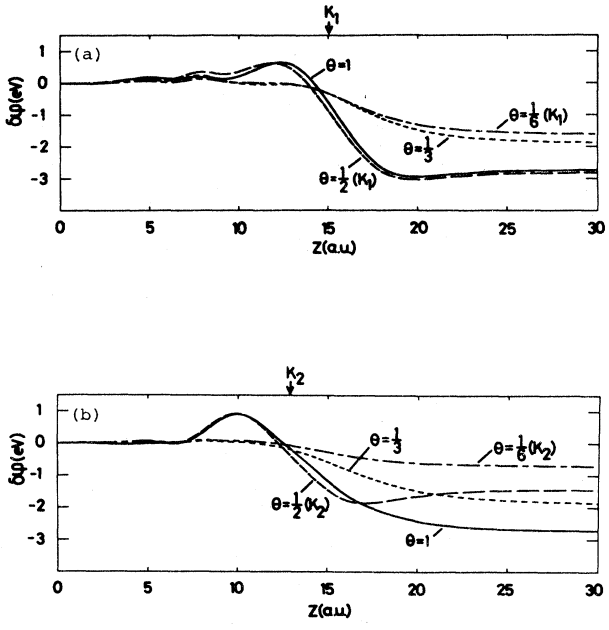

FIG. 13. The calculated change in the electrostatic potential $\delta\varphi(\mathbf{r},\Theta)$ along a vertical axis containing a K adatom at (a) K_1 site and (b) K_2 site. The work-function change $\Delta\Phi(\Theta)$ is read from its value at the vacuum. The arrow indicates the atomic position of K adatoms.

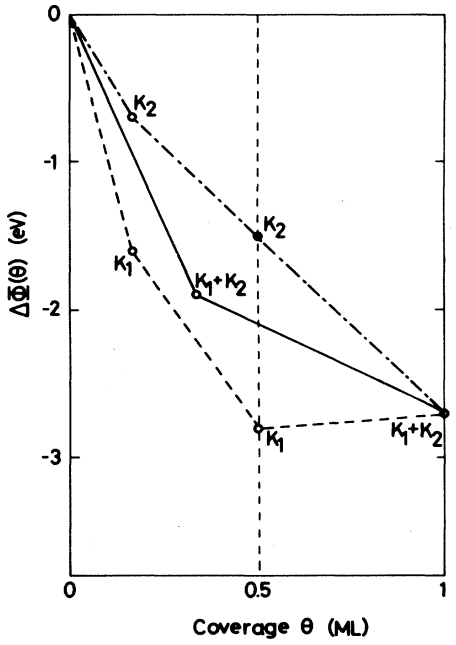

FIG. 14. The calculated work-function change $\Delta\Phi(\Theta)$ for the six overlayers.

Tochihara,[58] Enta *et al.*,[29] and Oellig and Miranda[59] were 3.3, 3.2, and 2.6 eV, respectively. The present results, 2.8 eV for $\Theta=\frac{1}{2}$ (K_1) and 2.7 eV for $\Theta=1$ (K_1+K_2) are in reasonable agreement with these experimental values. Thus we cannot assert the correct value for Θ_s definitely from the above results alone. Nevertheless, since $\Delta\Phi(\Theta)$ at $\Theta=\frac{1}{2}$ for the K_2 site is only half as much as experimental values, it is conclusive that K adatoms must sit on the top of Si dimers rather than valley sites between two dimer chains, if indeed $\Theta_s=\frac{1}{2}$. The reason why the dipole moment for K_2 is smaller than that for K_1 is easily understood from Figs. 11 and 12; the vertical separation between the center of gravity of the Si—K bond charge and that for the charge depletion area in the vacuum side of a K atom, which determines the length of the dipole moment, is much smaller for K_2 than for K_1.

We may discuss the preferred adsorption site of K atoms also from view points of adsorption energy. The adsorption energies of K atoms calculated as the total energy of K/Si(001) minus those of the isolated K layer and bare Si(001)-(2×1) are 3.3, 3.4, 2.5, and 2.6 eV for $\Theta=\frac{1}{6}$ (K_1), $\frac{1}{6}$ (K_2), $\frac{1}{2}$ (K_1), and $\frac{1}{2}$ (K_2), respectively. The value for the Levine model [$\Theta=\frac{1}{2}$ (K_1)] is in agreement with the value of Ciraci and Batra. Because of the neglect of the K 3*p* polarization in the present pseudopotential calculation, the above values might be overestimated to some extent, yet the difference for different sites and Θ values may be meaningful. The adsorption energies for $\Theta=\frac{1}{2}$ is considerably smaller than those at $\Theta=\frac{1}{6}$, one clear evidence of the weakening of the Si—K bonding with increasing Θ. On the other hand, there is no appreciable difference between the adsorption energy for K_1 and that for K_2 for a common Θ. (Although the above values for K_2 are a little larger than those for K_1, the order may be reversed depending on the actual Si-K distance.) Therefore one could not argue that either K_1 or K_2 alone is preferred as the adsorption site. If judged merely from the above values, the assumption that $\Theta_s=1$ seems more plausible. However, depending on the shape of the potential surface in the vacuum region for incoming K atoms, which was not considered in the present calculation, it might happen that K atoms comes down to sit on either site selectively. Further study is necessary in this regard.

As is seen from Fig. 14, the calculated work function for the present system does not show such a clear minimum before Θ_s unlike for most of metal substrates. This indicates that $d(\Theta)$ is not so rapidly reduced with increasing Θ as compared with the case of metal substrates. In the present calculation, $d(\Theta)$ at $\Theta=\frac{1}{2}$ for the K_1 site is $\sim 60\%$ of that at $\Theta=\frac{1}{6}$, while, in the previous calculation for Na/Al(001),[22] $d(\Theta)$ at $\Theta=\frac{1}{2}$ is only $\sim 35\%$ of that at $\Theta=\frac{1}{8}$. Of course, the 40% reduction of $d(\Theta)$ for the K_1 site indicates the smaller polarization of K adatoms, and thus, weaker bonding between Si and K atoms with increasing Θ, which follows the larger K-K interaction. However, its magnitude is smaller as compared with the case of metal substrates owing to the active Si dangling-bond states.

Another important quantity in Fig. 13 is the values of $\delta\varphi(\mathbf{r},\Theta)$ at the adatom sites. In previous theories based on the classical point-charge-transfer model,[12–14] it was assumed to be lowered by electron volts as Θ varies from low to full coverages, which was indispensable to make ionized adatoms at lower Θ neutralize with increasing Θ. However, as is seen from these figures, although $\delta\varphi(\mathbf{r},\Theta)$ at $z=\infty$ depends significantly on Θ, its values at the adsorption sites are rather insensitive to Θ; its variation with Θ is very small for K_2, and the maximum variation for K_1 is ~ 0.4 eV. Therefore, the large depolarization field as assumed in the classical Gurney model[11] is absent in the present system. This is consistent with the observation that the calculated adatom DOS is rather insensitive to Θ. Enta *et al.*[29] measured the *K* 3*p* and Cs 5*p* levels on Si(001) as a function of Θ, and found that their Θ dependence is quite small. Although understanding of the core levels requires the knowledge of final-state relaxations which might also depend on Θ, the absence of the large Θ dependence in the potential value at K sites found in the present calculation is in good accord with their observation.

E. On the nature of K overlayers at higher Θ

Adsorption of alkali metals on Si(001)-(2×1) originally attracted much attention in connection with realization of one-dimensional free-electron-like metals.[28] Later, Ciraci and Batra[34,35] claimed that alkali-metal adatoms are perfectly ionized on this surface and that surface metallization takes place through the partial filling of the Si dangling-bond states. The above two arguments may be regarded as giving two limiting cases, where the orbital interaction between the adatom and substrate states could be ignored. Here, we briefly discuss the origin of

the surface metallization at $\Theta=\frac{1}{2}$. (As was shown, the surface becomes semiconducting if $\Theta_s=1$.) First, we show in Figs. 15(a) and 15(b), the charge density of the isolated K monolayer at $\Theta=\frac{1}{2}$ which may be taken as a reference charge density corresponding to the former limit. [The vertical cut planes in the left-hand and right-hand sides of Fig. 15 are the same as those in Fig. 11(a) and 11(b), respectively.] There is little interaction between the neighboring K chains, and they have a one-dimensional metallic character with ample metallic bond charge in the nearest-neighbor K—K bonds. On the other hand, Figs. 15(c) and 15(d) show the difference in the charge density between the bare Si(001)-(2×1) and an artificial surface where one additional electron per unit cell is accommodated further into the S_1 and S_2 bands of the bare Si(001). It is based on the rigid band model, and therefore may give a reference charge density in the latter limit. In order to shed light onto the problem of whether the real surface is closer to either of the two limits, it may be useful to examine how the charge density of the additional one electron from an adatom actually distributes in the surface region. For this purpose, we show in Figs. 15(e) and 15(f) the difference in the charge density between the K/Si(001)-(2×1) at $\Theta=\frac{1}{2}$ (K_1) and bare Si(001) surfaces. [$\delta\rho(\mathbf{r},\Theta)$ in Fig. 12(a) is obtained as a difference between the charge densities in Fig. 15(a) and 15(e).] It becomes slightly negative in the substrate side due to the relocation of the Si charge density. It seems rather natural to conclude that the charge densities in Figs. 15(e) and 15(f) resemble those in Figs. 15(a) and 15(b) more closely than those in Figs. 15(c) and 15(d); although polarized toward the substrate side, one can still see in Fig. 15(f) as much bond charge in the nearest K—K bond as in Fig. 15(b), and also the outermost charge contour line around a K atom in Fig. 15(e) which extends considerably toward the vacuum may be associated with K valence states. Such an extension of the charge density toward the vacuum may be indispensable for the appearance of a sharp peak near E_F in MDS experiments as observed by Nishigaki *et al.*[39] Thus it may not be appropriate to claim that K atoms become *perfect* ions on the present surface. The strengthening of the nearest K—K bond with increasing Θ is also seen indirectly as a corresponding weakening of the Si—K bond; the calculated adsorption energy of a K atom at K_1 at $\Theta=\frac{1}{2}$ were $\sim 75\%$ of that at $\Theta=\frac{1}{6}$. However, at the same time, it is also misleading to claim that the K chains form one-dimensional metals, since, as shown before, there is no surface states in the Si gap with the free-electron-like dispersion.

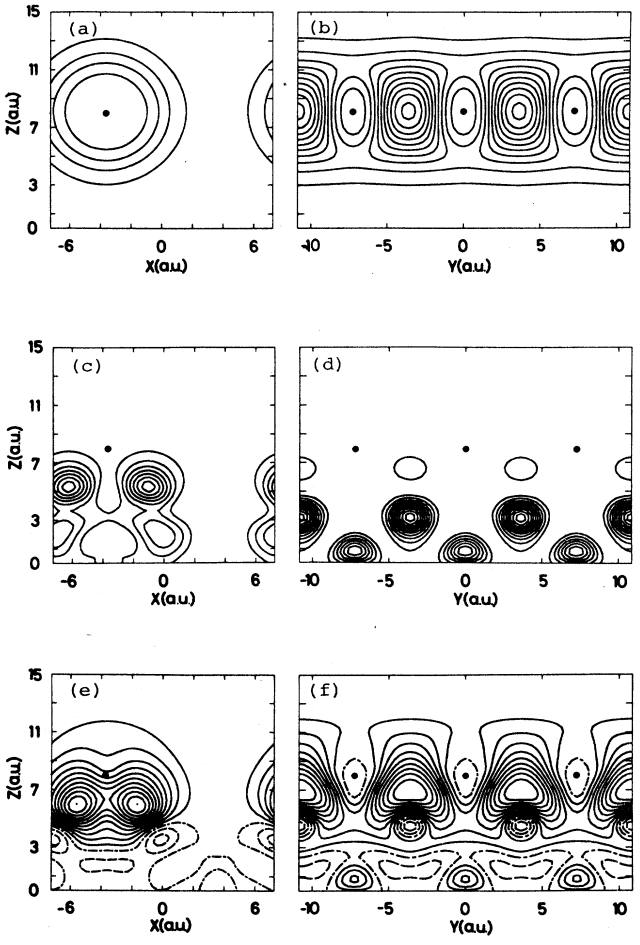

FIG. 15. (a) and (b) Contour maps of the total electron density of the isolated K layer for $\Theta=\frac{1}{2}$ (K_1). (c) and (d) Contour maps of the difference in the total electron density between the bare Si(001) surface and an artificial surface where one additional electron per unit cell is accommodated further into the S_1 and S_2 bands of the bare Si(001). (e) and (f) Contour maps of the difference in the total electron density between the K/Si(001)-(2×1) at $\Theta=\frac{1}{2}$ (K_1) and bare Si(001) surfaces. The vertical cut planes in the left-hand and right-hand sides are the same as those in Figs. 11(a) and 11(b), respectively.

IV. SUMMARY AND CONCLUSION

The electronic structure of K adatoms on the Si(001)-(2×1) surface was studied for a wide range of the adatom coverage (Θ) including lower Θ values where the direct interaction among adatoms is negligibly small. The K adatoms were assumed to sit on the raised site on the Si dimer chains (K_1), and also on the valley site between the two neighboring dimer chains (K_2). The surface electronic structure was calculated for six K overlayer configurations ranging from $\Theta=\frac{1}{6}$ to 1 in units of Si monolayers. The important results obtained are summarized as follows. (1) Even for high Θ values, no surface band with the free-electron-like dispersion appears in the Si gap region, and the two gap states, S_1 and S_2 (or $2N$ surface states which is made from S_1 and S_2 due to the folding of SBZ if the unit cell has a $2\times N$ structure as for $\Theta=\frac{1}{6}$ and $\frac{1}{3}$ in the present calculations) presistently exist, which is consistent with the previous study of Ciraci and Batra. (2) With increasing Θ, however, these gap states shift to higher binding energies with reference to the bulk states because of the kinetic energy lowering caused by the delocalization of their wave functions toward the overlayer regions. This aspect may be interpreted as a re-

sult of the Si-K hybridization (interface state). (3) The importance of the Si-K hybridization in the Si—K bonding is also clearly demonstrated from the calculated DOS in a K sphere where the peaks corresponding to the gap states are greatly enhanced upon K adsorption. (4) The filled part of the K DOS is rather insensitive to Θ, and it shows no drastic change as assumed in the classical model of Gurney. This is because the depolarization field is virtually absent at adatom sites because of the screening effect of the substrate. (5) The adatom is essentially neutral if the electron density is averaged in the adatom sphere even at low Θ, and the adatom dipole moment is caused by the modification of the dipole part of the electron density in the sphere, which may be interpreted as a polarization of adatoms due to the Si-K hybridization. (6) With increasing Θ, the K—K bonding is strengthened, which then leads to the weaker Si—K bonding, and thus, smaller K adsorption energy and smaller K adatom dipole moment. However, because of the active Si dangling-bond states, the weakening of the Si—K bond is not so signficant as in the case of metal substrates.

From the recent first-principles electronic structure calculations for the alkali-metal overlayers on simple and transition-metal substrates, a new picture for the adsorption has been deduced. In this model, the orbital hybridization between the adatom and substrate states plays a central role in the adatom-substrate bonding and adatom dipole moment for whole the Θ range. As described in the preceding paragraph, the present calculation showed that such a model may be also applicable for semiconductor substrates with active dangling bonds essentially without significant changes. This may be impressive since one might first expect that the screening of semiconductors is considerably less effective than that of metal substrates, and therefore that there may be a large depolarization field at adatom sites, which results in a large Θ dependence of the adatom charge state as assumed in the classical model.

ACKNOWLEDGMENTS

The authors are grateful to Professor M. Nakayama and Professor T. Kato for stimulating discussions. We are also indebted to Professor M. Tsukada, Dr. N. Shima, and Dr. Z. Zhu for the collaboration in the early stage of this work. The numerical calculations were performed at the computer centers of University of Tokyo, Institute for Solid State Physics, and Institute for Molecular Science. This work was partially supported by a Grant-in-Aid for Scientific Research on Priority Areas from Ministry of Education, Science, and Culture.

[1]K. H. Kingdon and I. Langmuir, Phys. Rev. **21**, 380 (1923).
[2]J. B. Taylor and I. Langmuir, Phys. Rev. **44**, 423 (1933).
[3]J. Topping, Proc. R. Soc. London, Ser. A **114**, 67 (1927).
[4]J. Cousty, R. Riwan, and P. Soukiassian, J. Phys. (Paris) **46**, 1693 (1985); S. A. Lindgren and L. Wallden, Phys. Rev. B **22**, 5969 (1980); U. Jostell, Surf. Sci. **82**, 333 (1979).
[5]A. U. MacRae, K. Muller, J. J. Lander, J. Morrison, and J. C. Phillips, Phys. Rev. Lett. **22**, 1048 (1969); A. U. MacRae, K. Muller, J. J. Lander, and J. Morrison, Surf. Sci. **15**, 483 (1969).
[6]H. Ishida and M. Tsukada, Surf. Sci. **169**, 225 (1986).
[7]D. Heskett, I. Strathy, E. W. Plummer, and R. A. de Paola, Phys. Rev. B **32**, 6222 (1985).
[8]W. Eberhardt, F. M. Hoffmann, R. de Paola, D. Heskett, I. Strathy, E. W. Plummer, and H. R. Moser, Phys. Rev. Lett. **54**, 1856 (1985).
[9]H. P. Bonzel, J. Vac. Sci. Technol. A **2**, 866 (1984).
[10]H. P. Bonzel, Surf. Sci. Rep. **8**, No. 2 (1988).
[11]R. W. Gurney, Phys. Rev. **47**, 479 (1935).
[12]J. P. Muscat and D. M. Newns, Solid State Commun. **11**, 737 (1972); J. Phys. C **7**, 2630 (1974).
[13]J. P. Muscat and I. P. Batra, Phys. Rev. B **34**, 2889 (1986).
[14]A. J. Benett, J. Chem. Phys. **49**, 1340 (1968); L. D. Schmidt and R. J. Gomer, **45**, 1605 (1966).
[15]N. D. Lang, Phys. Rev. B **4**, 4234 (1971).
[16]W. Ning, C. Kailai, and W. Dingsheng, Phys. Rev. Lett. **56**, 2759 (1986); R. Wu, K. Chen, D. Wang, and N. Wang, Phys. Rev. B **38**, 3180 (1988).
[17]P. A. Serena and N. Garcia, Surf. Sci. **189/190**, 232 (1987).
[18]P. A. Serena, J. M. Soler, N. Garcia, and I. P. Batra, Phys. Rev. B **36**, 3452 (1987).
[19]H. Ishida and K. Terakura, Phys. Rev. B **36**, 4510 (1987).
[20]H. Ishida, Phys. Rev. B **38**, 8006 (1988).
[21]H. Ishida, Phys. Rev. B **39**, 5492 (1989); **40**, 1341 (1989).
[22]H. Ishida and K. Terakura, Phys. Rev. B **38**, 5752 (1988).
[23]E. Wimmer, A. J. Freeman, M. Weinert, H. Krakauer, J. R. Hiskes, and A. M. Karo, Phys. Rev. Lett. **48**, 1128 (1982).
[24]E. Wimmer, A. J. Freeman, J. R. Hiskess, and A. M. Karo, Phys. Rev. B **28**, 3074 (1983).
[25]S. R. Chubb, E. Wimmer, A. J. Freeman, J. R. Hiskes, and A. M. Karo, Phys. Rev. B **36**, 4112 (1987).
[26]P. Soukiassian, R. Riwan, J. Lecante, E. Wimmer, S. R. Chubb, and A. J. Freeman, Phys. Rev. B **31**, 4911 (1985).
[27]J. D. Levine, Surf. Sci. **34**, 90 (1973).
[28]T. Aruga, H. Tochihara, and Y. Murata, Phys. Rev. Lett. **53**, 372 (1984).
[29]Y. Enta, T. Kinoshita, S. Suzuki, and S. Kono, Phys. Rev. B **36**, 9801 (1987); **39**, 1125 (1989).
[30]T. Abukawa and S. Kono, Phys. Rev. B **37**, 9097 (1988); T. Abukawa, S. Kono, and T. Sakamoto, Jpn. J. Appl. Phys. **28**, L303 (1989).
[31]A. Ichimiya and S. Kohmoto (unpublished).
[32]I. P. Batra, Phys. Rev. B **39**, 3919 (1989).
[33]H. Ishida, N. Shima, and M. Tsukada, Phys. Rev. B **32**, 6246 (1985); Surf. Sci. **158**, 438 (1985).
[34]S. Ciraci and I. P. Batra, Phys. Rev. Lett. **56**, 877 (1986).
[35]S. Ciraci and I. P. Batra, Phys. Rev. B **37**, 2955 (1988).
[36]T. Kendelewicz, P. Soukiassian, R. S. List, J. C. Woicik, P. Pianetta, I. Lindau, and W. E. Spicer, Phys. Rev. B **37**, 7115 (1988).
[37]R. V. Kasowski and M. H. Tsai, Phys. Rev. Lett. **60**, 546 (1988).
[38]P. Soukiassian and T. Kendelewicz, in *Proceeding of the NATO Advanced Research Workshop on Metallization and*

Metal-Semiconductor Interfaces, Garching, 1988, edited by I. P. Batra (Plenum, New York, 1988), p. 465.

[39]S. Nishigaki, S. Matsuda, T. Sakaki, N. Kawanishi, and A. Kawase, (unpublished); see also, S. Nishigaki, N. Oishi, S. Matsuda, N. Kawanishi, and T. Sakai, Phys. Rev. B **39**, 8048 (1989).

[40]K. Horn, A. Hohlfeld, J. Somers, Th. Linder, P. Hollins, and A. M. Bradshaw, Phys. Rev. Lett. **61**, 2488 (1988); D. Heskett, K.-H. Frank, E. E. Koch, and H.-J. Freund, Phys. Rev. B **36**, 1276 (1987).

[41]G. A. Benesh, H. Krakauer, and U. E. Ellis, and M. Posternak, Surf. Sci. **104**, 599 (1981); G. A. Benesh and J. R. Hester, *ibid.* **194**, 567 (1988).

[42]P. Hohenberg and W. Kohn, Phys. Rev. **136**, B864 (1964); W. Kohn and L. J. Sham, *ibid.* **140**, A1133 (1965).

[43]G. B. Bachelet, D. R. Hamann, and M. Schlüter, Phys. Rev. B **26**, 4199 (1982).

[44]D. J. Chadi, Phys. Rev. Lett. **43**, 43 (1979); M. T. Yin and M. L. Cohen, Phys. Rev. B **24**, 2303 (1981).

[45]M. Tsukada, N. Shima, Z. Zhu, H. Ishida, and K. Terakura, in Ref. 38, p. 351.

[46]M. C. Asensio, E. G. Michel, J. Alvarez, C. Ocal, R. Miranda, and S. Ferrer, Surf. Sci. **211/212**, 31 (1989).

[47]M. T. Yin and M. L. Cohen, Phys. Rev. B **26**, 5668 (1982).

[48]J. Ihm, M. L. Cohen, and D. J. Chadi, Phys. Rev. B **21**, 4592 (1980).

[49]P. Kruger and J. Pollmann, Phys. Rev. B **38**, 10 578 (1988).

[50]Y. Enta, S. Suzuki, S. Kono, and T. Sakamoto, Phys. Rev. B **39**, 5524 (1989).

[51]Y. Murata, H. Tochihara, and M. Kubota, in Ref. 38, p. 367.

[52]H. Tochihara, Surf. Sci. (to be published).

[53]V. Heine, in *Solid State Physics,* edited by H. Ehrenreich, F. Seitz, and D. Turnbull (Academic, New York, 1980), Vol. 35.

[54]For example, H. Ibach and D. L. Mills, *Electron Energy Loss Spectroscopy and Surface Vibrations* (Academic, New York, 1982).

[55]D. M. Newns, Phys. Lett. **38A**, 341 (1972); M. Nakayama, T. Kato, and K. Ohtomi, Solid State Commun. **50**, 409 (1984).

[56]See, for example, J. P. Muscat and D. M. Newns, Prog. Surf. Sci. **9**, 1 (1978); N. D. Lang, in *Theory of the Inhomogeneous Electron Gas,* edited by S. Lundqvist and N. H. March (Plenum, New York, 1983).

[57]N. D. Lang and A. R. Williams, Phys. Rev. B **18**, 615 (1978); **16**, 2408 (1977).

[58]H. Tochihara (private communication).

[59]E. M. Oelling and R. Miranda, Surf. Sci. **177**, L947 (1986).